J|A|C|S
ARTICLES

Published on Web 09/06/2008

Low Coordinate, Monomeric Molybdenum and Tungsten(III) Complexes: Structure, Reactivity and Calculational Studies of $(silox)_3Mo$ and $(silox)_3ML$ (M = Mo, W; L = PMe_3, CO; silox = $^tBu_3SiO$)

David S. Kuiper,[†] Peter T. Wolczanski,*[,†] Emil B. Lobkovsky,[†] and Thomas R. Cundari*[,‡]

Department of Chemistry and Chemical Biology, Baker Laboratory, Cornell University, Ithaca, New York 14853, and Department of Chemistry, Center for Advanced Scientific Computing and Modeling (CASCaM), P.O. Box 305070, University of North Texas, Denton, Texas 76203

Received April 21, 2008; E-mail: ptw2@cornell.edu (P.T.W.); tomc@unt.edu (T.R.C.)

Abstract: Treatment of $(silox)_3MCl$ (M = Mo, **1**-Cl; W, **2**-Cl; silox = $^tBu_3SiO$) with PMe_3 and Na/Hg led to formation of monomeric, d^3 phosphine adducts, $(silox)_3MPMe_3$ (M = Mo, **1**-PMe_3; W, **2**-PMe_3) via $(silox)_3ClMPMe_3$ (M = Mo, **1**-$ClPMe_3$; W, **2**-$ClPMe_3$). Structural studies show **1**-PMe_3 and **2**-PMe_3 to be highly distorted; calculations on full chemical models corroborate experimentally determined $S = {}^1/_2$ ground states and their structural features. The compounds contain a bent M-P bond that is characteristic of significant σ/π-mixing. PMe_3 may be thermally removed from **1**-PMe_3 *in vacuo* to produce $^4A_2'$ $(silox)_3Mo$ (**1**), which was derivatized with CO, NO, and 1/4 P_4 to form $(silox)_3Mo$ (**1**-CO), $(silox)_3MoNO$ (**1**-NO), and $(silox)_3MoP$ (**1**-P), respectively. Calculations revealed $(silox)_3W$ (**2′**) to have an $S = {}^1/_2$ ground state, which may render it too reactive to be isolated. Treatment of **2**-PMe_3 with CO, NO, and 1/4 P_4 formed $(silox)_3WCO$ (**2**-CO), $(silox)_3WNO$ (**2**-NO), and $(silox)_3WP$ (**2**-P), respectively. **2**-CO and **2**-NO are more conveniently prepared from Na/Hg reductions of **2**-Cl in the presence of CO and NO, respectively. Calculations reveal subtle effects of $nd_{z^2}/(n+1)s$ mixing in differentiating the chemistry of Mo and W and in rationalizing the generation of mononuclear species.

Introduction

Studies in these laboratories have focused on elucidating the electronic features of second and third row transition elements that distinguish their structure and reactivity patterns within a group. Previous investigations focusing on comparisons of d^2 species in groups 5[1,2] and 6[3] revealed that $nd_{z^2}/(n+1)s$ mixing can have a profound influence on their chemistry.[4,5] Orbital symmetry requirements prevent ready oxygen atom transfer involving $(silox)_3M$ (M = NbL (L = PMe_3, 4-pic), Ta),[1] and olefin substitutions in $(silox)_3M(ole)$ (M = Nb, Ta) exhibit different linear free energy relationships dependent on the density of states along the reaction coordinate.[2] More recently, profound structural differences have been observed for $(silox)_3MX$ (M = Mo, X = Cl, Et; M = W, X = Cl, Me); trigonal monoyramidal (pseudo T_d) molybdenum derivatives differ substantially from the squashed tetrahedral (distorted square planar) conformations of the corresponding tungsten compounds.[3]

In an effort to extend these comparative studies to other d^n species, low-coordinate, monomeric derivatives of d^3 Mo(III) and W(III) were sought. In group 6, the metal−metal triple bond has historically been a formidable thermodynamic sink that needs to be overcome for molybdenum and tungsten.[6] Despite the use of the silox ($^tBu_3SiO$) ligand, a bulky pseudohalide that has enabled the synthesis of numerous low coordinate compounds,[1,7−13] initial attempts to synthesize mononuclear M(III) derivatives failed to thwart triple bond formation. Certain aspects

[†] Cornell University.
[‡] CASCaM.

(1) Veige, A. S.; Slaughter, L. M.; Lobkovsky, E. B.; Wolczanski, P. T.; Matsunaga, N.; Decker, S. A.; Cundari, T. R. *Inorg. Chem.* **2003**, *42*, 6204–6224.
(2) Hirsekorn, K. F.; Hulley, E. B.; Wolczanski, P. T.; Cundari, T. R. *J. Am. Chem. Soc.* **2008**, *130*, 1183–1196.
(3) Kuiper, D. S.; Douthwaite, R. E.; Mayol, A.-R.; Wolczanski, P. T.; Lobkovsky, E. B.; Cundari, T. R.; Lam, O. P.; Meyer, K. *Inorg. Chem.* **2008**, *47*, 7139–7153.
(4) (a) Firman, T. K.; Landis, C. R. *J. Am. Chem. Soc.* **2001**, *123*, 11728–11742. (b) Landis, C. R.; Cleveland, T.; Firman, T. K. *J. Am. Chem. Soc.* **1998**, *120*, 2641–2649. (c) Landis, C. R.; Firman, T. K.; Root, D. M.; Cleveland, T. *J. Am. Chem. Soc.* **1998**, *120*, 1842–1854. (d) Weinhold, F.; Landis, C. R. *Valency and Bonding*; Cambridge University Press: Cambridge, 2005. (e) For a convenient plot of orbital energies vs. Z, see Figure 15.39 in: Oxtoby, D. W.; Gillis, H. P.; Nachtrieb, N. H. *Principles of Modern Chemistry*, 5th ed.; Thomson Brooks/Cole: United States, 2002.
(5) Pyykko, P. *Chem. Rev.* **1988**, *88*, 563–594.
(6) (a) Cotton, F. A.; Walton, R. A. *Multiple Bonds Between Metal Atoms*; Oxford University Press: New York, 1993. (b) Chisholm, M. H. *Acc. Chem. Res.* **1990**, *23*, 419–425. (c) Chisholm, M. H.; Cotton, F. A. *Acc. Chem. Res.* **1978**, *11*, 356–362.
(7) Covert, K. J.; Neithamer, D. R.; Zonnevylle, M. C.; LaPointe, R. E.; Schaller, C. P.; Wolczanski, P. T. *Inorg. Chem.* **1991**, *30*, 2494–2508.
(8) (a) Neithamer, D. R.; LaPointe, R. E.; Wheeler, R. A.; Richeson, D. S.; Van Duyne, G. D.; Wolczanski, P. T. *J. Am. Chem. Soc.* **1989**, *111*, 9056–9072. (b) Chadeayne, A. R.; Wolczanski, P. T.; Lobkovsky, E. B. *Inorg. Chem.* **2004**, *43*, 3421–3432.
(9) Sydora, O. L.; Wolczanski, P. T.; Lobkovsky, E. B.; Buda, C.; Cundari, T. R. *Inorg. Chem.* **2005**, *44*, 2606–2618.

Scheme 1

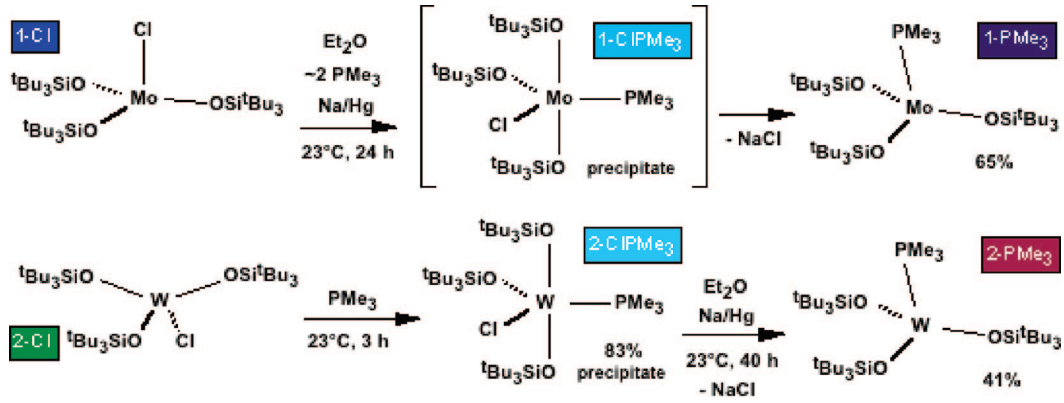

of this chemistry—such as CO dissociation across the ditungsten bond of $(silox)_2ClW{\equiv}WCl(silox)_2$[14] to give $(silox)_2(O)W{=}C{=}WCl_2(silox)_2$,[15] and ethylene cleavage by the putative $[(silox)_2W]_2$ to provide transient $[(silox)_2W]_2(\mu\text{-}CH)(\mu\text{-}CH_2)(\mu\text{-}H)$ en route to $[(silox)_2W]_2(\mu\text{-}CH)_2$ and dihydrogen[16]—proved to be intriguing, but most of the structure and reactivity studies followed established patterns.[6] A switch to the amide ligand, ^{t}Bu$_3$SiNH, permitted cleavage of $(^t\text{Bu}_3\text{SiNH})_2ClW{=}WCl(HNSi^t\text{Bu}_3)_2$ via NH bond activation, but stable products of the degradation were all W(VI).[17]

Recently, different procedures led to the synthesis of $(silox)_3MCl$ (M = Mo, W),[3] the first instance in which the *tris*-silox coordination sphere was attained for the 4d and 5d metals of group 6. As described below, reductions of the M(IV) (M = Mo, W) halides enabled the synthesis of rare mononuclear M(III) complexes of group 6, including $(silox)_3Mo$. In addition to their chemistry, evaluation of the compounds via calculations provides considerable insight, especially with regard to the influence of $nd_{z^2}/(n+1)s$ mixing.[4,5]

Results

Syntheses of $(silox)_3MPMe_3$ (M = Mo, 1-PMe$_3$; W, 2-PMe$_3$). As illustrated in Scheme 1, the syntheses of $(silox)_3MPMe_3$ (M = Mo, **1**-PMe$_3$; W, **2**-PMe$_3$) were accomplished via Na/Hg reductions in the presence of PMe_3. Upon admission of an excess of PMe_3 to blue Et_2O solutions of trigonal monoyramidal $(silox)_3MoCl$ (**1**-Cl),[3] an aqua-blue precipitate appeared immediately, and the solution became virtually colorless, implicating the generation of $(silox)_3ClMoPMe_3$ (**1**-ClPMe$_3$). Reduction to Mo(III) occurred over 24 h, and purple **1**-PMe$_3$ was isolated upon crystallization from Et_2O. The ^{1}H NMR spectrum of **1**-PMe$_3$ consists of broad singlets at δ 1.51 ($\nu_{1/2}$ = 20 Hz) and δ 2.62 ($\nu_{1/2}$ = 48 Hz) observed in a 9:1 ratio, and its ^{13}C {^{1}H} NMR spectrum showed only broad silox resonances at 39.1 (CH_3) and 137 (SiC) ppm. An Evans' method[18] measurement revealed a μ_{eff} of 2.0 μ_B, consistent with the expected doublet ground state.

The preparation of $(silox)_3WPMe_3$ was similar to that of the molybdenum analogue, except that squashed-T_d $(silox)_3WCl$ (**2**-Cl)[3] appeared to be quite prone to over-reduction. After one-pot procedures proved finicky, **2**-Cl was first converted to the aqua-blue PMe_3 adduct $(silox)_3ClWPMe_3$ (**2**-ClPMe$_3$) in 83% yield. A ^{1}H NMR spectrum of a faintly colored C_6D_6 solution of $(silox)_3ClWPMe_3$ (**2**-ClPMe$_3$) revealed two low intensity paramagnetic resonances in a 2:1 ratio hence the tbp structure illustrated in Scheme 1 has been tentatively assigned to both phosphine adducts. Only a 5% excess of Na was used in the subsequent Na/Hg reduction of **2**-ClPMe$_3$, which occurred over a 40 h period at 23 °C. Crystallization from Et_2O/PMe_3 resulted in the isolation of the burgundy W(III) phosphine complex, $(silox)_3WPMe_3$ (**2**-PMe$_3$), in 41% yield. ^{1}H NMR spectroscopy of **2**-PMe$_3$ revealed broad resonances at δ 1.31 ($\nu_{1/2} \approx$ 37 Hz) and δ 12.77, and integration of the latter (~5 H) very broad resonance ($\nu_{1/2} \approx$ 950 Hz) leaves its assignment as the PMe_3 group somewhat tenuous. The μ_{eff} was 1.7 μ_B according to an Evans' method[18] measurement, again consistent with a doublet ground state.

Structures of $(silox)_3MPMe_3$ (M = Mo, 1-PMe$_3$; W, 2-PMe$_3$). Table 1 provides information about the data collection and refinement of single crystal X-ray structure determinations of $(silox)_3MPMe_3$ (M = Mo, **1**-PMe$_3$; W, **2**-PMe$_3$), while pertinent bond distances and angles are given in Table 2. The structure of $(silox)_3NbPMe_3$ manifested a C_{3v} geometry consistent with the $^3A_2$ ground state.[1] It was questionable whether a significant Jahn−Teller distortion[19] would disrupt a C_{3v} conformation and the corresponding ^{3}E ground-state of d^3 **1**-PMe$_3$ or **2**-PMe$_3$ given the π-type character (i.e., O-M π^*; P-M π^b) of the $(d_{xz}d_{yz})^3$ electronic configuration. As the data in Table 2, and the illustrations in Figures 1 and 2, show, the distortion is extreme, and additional low symmetry features are present.

Figure 1a shows the molecular skeleton of $(silox)_3MoPMe_3$ (**1**-PMe$_3$). Its squashed tetrahedral geometry features one open O−Mo−O angle of 132.71(7)° and normal 110.89(7)° and

(10) Veige, A. S.; Wolczanski, P. T.; Lobkovsky, E. B. *J. Chem. Soc., Chem. Commun.* **2001**, 2734–2735.
(11) Sydora, O. L.; Kuiper, D. S.; Wolczanski, P. T.; Lobkovsky, E. B.; Dinescu, A.; Cundari, T. R. *Inorg. Chem.* **2006**, *45*, 2008–2021.
(12) Rosenfeld, D. C.; Wolczanski, P. T.; Barakat, K. A.; Buda, C.; Cundari, T. R.; Schroeder, F. C.; Lobkovsky, E. B. *Inorg. Chem.* **2007**, *46*, 9715–9735.
(13) Eppley, D. F.; Wolczanski, P. T. *Angew. Chem., Int. Ed. Engl.* **1991**, *30*, 584–585.
(14) Miller, R. L.; Lawler, K. A.; Bennett, J. L.; Wolczanski, P. T. *Inorg. Chem.* **1996**, *35*, 3242–3253.
(15) Miller, R. L.; Wolczanski, P. T.; Rheingold, A. L. *J. Am. Chem. Soc.* **1993**, *115*, 10422–10423.
(16) Chamberlin, R. L. M.; Rosenfeld, D. C.; Wolczanski, P. T.; Lobkovsky, E. B. *Organometallics* **2002**, *21*, 2724–2735.
(17) Holmes, S. M.; Schafer II, D. F.; Wolczanski, P. T.; Lobkovsky, E. B. *J. Am. Chem. Soc.* **2001**, *123*, 10571–10583.
(18) (a) Evans, D. F. *J. Chem. Soc.* **1959**, 2003–2005. (b) Schubert, E. M. *J. Chem. Educ.* **1992**, *69*, 62.
(19) Figgis, B. N.; Hitchman, M. A. *Ligand Field Theory and Its Applications*; Wiley-VCH: New York, 2000.

Table 1. Crystallographic Data for $(silox)_3MoPMe_3$ (**1**-PMe_3), $(silox)_3WPMe_3$ (**2**-PMe_3), and $(silox)_3WCO$ (**2**-CO)

	1-PMe_3	2-PMe_3[a]	2-CO
formula	$C_{39}H_{90}O_3Si_3PMo$	$C_{39}H_{90}O_3Si_3PW$	$C_{37}H_{81}O_4Si_3W$
formula wt	818.32	906.23	858.16
space group	*C*2/*c*	$P\bar{1}$	$P2_1/n$
Z	8	4	4
a, Å	23.422(3)	12.9564(11)	8.68492)
b, Å	12.7232(14)	20.4690(17)	21.091(4)
c, Å	33.774(4)	21.6634(17)	24.354(5)
α, deg	90	63.760(4)	90
β, deg	108.588(2)	80.022(4)	94.12(3)
γ, deg	90	76.894(4)	90
V, Å^3	9539.6(18)	5001.4(7)	4449.0(15)
r_{calc}, g·cm^{-3}	1.140	1.203	1.281
μ, mm^{-1}	0.414	2.443	2.709
T, K	173(2)	173(2)	173(2)
λ (Å)	0.71073	0.71073	0.71073
R indices $[I > 2\sigma(I)]^{b,c}$	$R_1 = 0.0381$	$R_1 = 0.0322$	$R_1 = 0.0368$
	$wR_2 = 0.0901$	$wR_2 = 0.0725$	$wR_2 = 0.0865$
R indices (all data)^{b,c}	$R_1 = 0.0609$	$R_1 = 0.0528$	$R_1 = 0.0477$
	$wR_2 = 0.0971$	$wR_2 = 0.0764$	$wR_2 = 0.0912$
GOF[d]	1.034	1.066	1.107

[a] Two molecules (formulas) per asymmetric unit. [b] $R_1 = \Sigma||F_o| - |F_c||/\Sigma|F_o|$. [c] $wR_2 = [\Sigma w(|F_o| - |F_c|)^2/\Sigma wF_o^2]^{1/2}$. [d] *GOF* (all data) $= [\Sigma w(|F_o| - |F_c|)^2/(n - p)]^{1/2}$, n = number of independent reflections, p = number of parameters.

109.71(7)° angles. Figures 1a and 1b reveal the PMe_3 ligand tipped toward this opening, with ∠P1−Mo−O3 = 105.19(6)° in comparison to 93.97(5)° (∠P1−Mo−O1) and 97.91(5)° (∠P1−Mo−O2). The asymmetry of the system extends to the orientation of the phosphine, which is canted with respect to the Mo−P1 axis as Figure 1b indicates.[12] The P−CH_3 bond that is above O1−Mo−O2 has a C−P1−Mo angle of 123.19(10)° in contrast to the remaining C−P1−Mo angles of 113.00(9)° and 114.06(9)°, indicating that the 3-fold axis of the PMe_3 ligand is pointed slightly away from O3. The d(MoO) of 1.921(10) Å (ave), and the Mo−P1 distance of 2.3318(6) Å are consistent with a reduced Mo center.[12]

The X-ray crystal structure determination of $(silox)_3WPMe_3$ (**2**-PMe_3) revealed two independent molecules per asymmetric unit, with one possessing a ^{t}Bu group disorder. Both molecules are similar in conformation to **1**-PMe_3, but differ from one another enough to suggest that the potential energy surface of **2**-PMe_3 is relatively flat in response to subtle angular distortions. The molecules display tungsten−oxygen distances (1.902(12) Å (ave), 1.919(19) Å (ave)) appropriate for W(III), although the W−P bond length in the "less squashed" molecule (2.3685(5) Å) is longer than that of the molecule that resembles the Mo analogue (2.3346(6) Å). One molecule of **2**-PMe_3 possesses a O−W−O angle decidedly greater (138.77(5)°) than the other two (106.00(5)°, 107.14(5)°), and the phosphine leans into this opening (∠P2−W2−O5 = 123.79(4)°). The remaining P−W−O angles of 91.04(4)° and 90.45(4)° are much closer to the square planar norm than a tetrahedron. The PMe_3 is again oriented away from the W−P axis and toward O4−W2−O6 with C−P2−W2 angles that are 113.40(7)°, 113.74(7)°, and 124.42(8)°; the methyl corresponding to the last angle overhangs the opening as in **1**-PMe_3.[12]

The second molecule (Figure 2a) of $(silox)_3WPMe_3$ (**2**-PMe_3) is similarly distorted, but without the rough plane of symmetry evident in the first. One O−W−O angle is wider (125.75(6)°) than the others (108.33(5)°, 114.47(6)°), but the three are asymmetric. The phosphine again leans, but in this case it is more toward O1 (93.59(5)°) than toward O2 (100.11(6)°) or O3 (111.80(5)°). Figure 2b illustrates the cores of the two independent molecules with the tungstens, phosphorus atoms and O1/O4 placed in overlapping positions.

Calculations. 1. $(silox)_3MoPMe_3$ (1-PMe_3). Hybrid DFT/MM calculations[20−25] have been performed on full chemical models of $(silox)_3MoPMe_3$ (**1**-PMe_3) for both doublet and quartet ground states of the molecule (primes indicate calculated models). Table 2 reveals a strong correspondence between the calculated $S = 1/2$ ground state (^{2}**1′**-PMe_3) and that of the crystal structure. The $S = 3/2$ state was calculated to be within 3 kcal/mol of the doublet state, yet its geometry is trigonal monopyramidal[10,26] (∠P−Mo−O = 90°, ∠O−Mo−O = 120°), and the d(Mo−P) was calculated to be an unrealistic 3.03 Å, hence it was discounted as a viable ground-state species. The calculation of ^{2}**1′**-PMe_3 manifests the unusual structural features elaborated on above. The phosphine (∠O−Mo−*P* = 121.8°) is tipped into the wide O−Mo−O angle of 136.2°, and the PMe_3 unit is asymmetrically bound, with one Mo−P−C angle (120.6°) greater than the other two (115.8°, 117.1°).

Figure 3 provides illustrations and energies of the ligand field orbitals pertaining to ^{2}**1′**-PMe_3, the calculated model of $(silox)_3MoPMe_3$ (**1**-PMe_3). The low symmetry of the "squashed tetrahedron" renders the d-orbitals somewhat mixed, but traditional assignments can be made. Although problems with the Kohn−Sham orbital approximation limit the accuracy of orbital energies, especially those of filled vs half-filled vs virtual d-orbitals,[9,27] a rough "3 over 2" tetrahedral orbital manifold can be identified. A large d_{xz}/d_{yz} splitting of ∼0.76 eV accounts for part of the impetus toward the distorted structure, and reveals that $(d_{xz})^2$ is lower in energy than (d_{yz}),[1] and mixed with d_{z^2}. The orbital is primarily "d_{xz}", but its d_{z^2} character helps maximize Mo(d)→P(d/*σ**) backbonding while attenuating the O(p*π*)→Mo(d*π*) antibonding interaction. It is d_{yz} that carries the brunt of the metal−oxygen antibonding interactions in the z-direction, while the unoccupied $d_{x^2-y^2}$ and d_{xy} orbitals are Mo−O *π*-antibonding in the xy-plane in addition to being primarily Mo−O *σ** in character. The view down the P-M bond in "d_{z^2}" illustrates a bulge toward the O−Mo−O opening that reflects the antibonding component pertaining to the 3-orbital mixing of the P "lone pair" orbital, d_{xz} and d_{z^2}. The asymmetry of the Mo−P "bent" bond is thus due to *σ*/*π*-mixing.[12]

2. $(silox)_3WPMe_3$ (2-PMe_3). Figure 3 also illustrates the orbital energies of a model of $(silox)_3WPMe_3$ (**2**-PMe_3) that corresponds to the molecule whose metric parameters in Table 2 are associated with W2. The "less squashed" structure containing W1 is calculated to be lower in energy by 0.4 kcal/mol (i.e., the same energy within error limits of the computational models), but the former structure was found from both a global conformational search and one starting

(20) Frisch, M. J. Gaussian 03, revision C.02; Gaussian, Inc.: Wallingford, CT, 2004.
(21) Parr, R. G.; Yang, W. *Density-functional Theory of Atoms and Molecules*; Oxford Univ. Press: Oxford, 1989.
(22) Stevens, W. J.; Krauss, M.; Basch, H.; Jasien, P. G. *Can. J. Chem.* **1992**, *70*, 612–630.
(23) Hirsekorn, K. F.; Veige, A. S.; Marshak, M. P.; Koldobskaya, Y.; Wolczanski, P. T.; Cundari, T. R.; Lobkovsky, E. B. *J. Am. Chem. Soc.* **2005**, *127*, 4809–4830.
(24) Vreven, T.; Morokuma, K. *J. Comput. Chem.* **2000**, *21*, 1419–1432.
(25) Rappé, A. K.; Casewit, C. J.; Colwell, K. S.; Goddard, K. S.; Skiff, W. M. *J. Am. Chem. Soc.* **1992**, *114*, 10024–10035.
(26) Cummins, C. C.; Lee, J.; Schrock, R. R. *Angew. Chem., Int. Ed. Engl.* **1992**, *31*, 1501–1503.
(27) Zhang, G.; Musgrave, C. B. *J. Phys. Chem. A* **2007**, *111*, 1554–1561.

Table 2. Selected Bond Distances (Å) and Angles (deg) for $(silox)_3MoPMe_3$ (**1**-PMe_3), $(silox)_3WPMe_3$ (**2**-PMe_3), and $(silox)_3WCO$ (**2**-CO)[a]

	1-PMe_3	**1′**-PMe_3 ($S = {}^1/_2$)[b]	**2**-PMe_3[c]	**2′**-PMe_3 ($S = {}^1/_2$)[d]	**2**-CO
M−O1	1.9229(15)	1.962	1.9077(13)	1.936	1.889(2)
M−O2	1.9208(15)	1.976	1.9091(13)	1.967	1.887(2)
M−O3	1.9304(16)	1.986	1.8880(12)	1.967	1.868(2)
W2−O4			1.9232(11)	*1.928*	
W2−O5			1.8980(10)	*1.967*	
W2−O6			1.9345(13)	*1.983*	
M−P/C	2.3318(6)	2.434	2.3346(6), 2.3685(5)	2.397, *2.430*	1.892(4)
$(P-C)_{av}$	1.818(10)	1.889(14)	1.823(12)	1.896(17), *1.892(18)*	
$(O-Si)_{ave}$	1.635(5)	1.705(8)	1.643(6), 1.646 (8)	1.706(7), *1.710(8)*	1.667(3)
CO					1.174(5)
O1−M−O2	132.71(7)	136.2	125.75(6)	132.7	111.25(11)
O1−M−O3	110.89(7)	112.3	114.47(6)	110.1	113.26(11)
O2−M−O3	109.71(7)	104.8	108.33(5)	108.2	117.63(11)
O4−W2−O5			106.00(5)	*104.1*	
O4−W2−O6			138.77(5)	*137.4*	
O5−W2−O6			107.14(5)	*111.5*	
O1-M−P1/C	93.97(5)	86.6	93.59(5)	91.2	105.85(14)
O2−M−P1/C	97.91(5)	93.2	100.11(6)	93.2	105.46(13)
O3−M−P1/C	105.19(6)	121.8	111.80(5)	119.5	101.88(14)
O4−W2−P2			91.04(4)	*92.3*	
O5−W2−P2			123.79(4)	*125.8*	
O6−W2−P2			90.45(4)	*85.6*	
M−P−C	113.00(9)	115.8	113.75(7), 113.40(7)	113.2, *114.7*	
M−P−C	114.06(9)	117.1	117.12(8), 113.74(7)	115.1, *115.4*	
M−P−C	123.19(10)	120.6	121.64(8), 124.42(8)	126.1, *124.0*	
$(C-P-C)_{av}$	101.2(14)	100.0(31)	100.6(16)	99.5(18), *99.8(29)*	
M−O1−Si1	156.19(10)	154.3	165.14(10)	156.9	162.2(2)
M−O2−Si2	170.20(11)	155.1	162.70(11)	158.5	159.2(2)
M−O3−Si3	170.39(11)	155.5	169.74(11)	159.9	172.2(2)
W2−O4−Si4			158.39(9)	*154.1*	
W2−O5−Si5			158.91(8)	*154.6*	
W2−O6−Si6			158.61(8)	*154.7*	

[a] Calculated values (**1′**-PMe_3, **2′**-PMe_3) are given for optimized doublet ground states. [b] $\Delta H_{QD} = H(S = {}^3/_2) - H(S = {}^1/_2) = 2.6$ kcal/mol; the calculated quartet geometry is trigonal monopyramidal, and none of the metric parameters are close to observed. [c] Two independent molecules of **2**-PMe_3 are in the asymmetric unit; a disordered silox group is in one of the molecules. When two distances/angles are listed, the first is for W1, the second for W2. [d] $\Delta H_{QD} = H(S = {}^3/_2) - H(S = {}^1/_2) = 10.7$ kcal/mol. Starting from the geometries in the crystal structures, minima were found with reasonable correspondence to the observed conformations; the *italicized* geometry corresponds to the "more squashed" W2 structure, and it is 0.4 kcal/mol above the other. This geometry was also obtained from a global search.

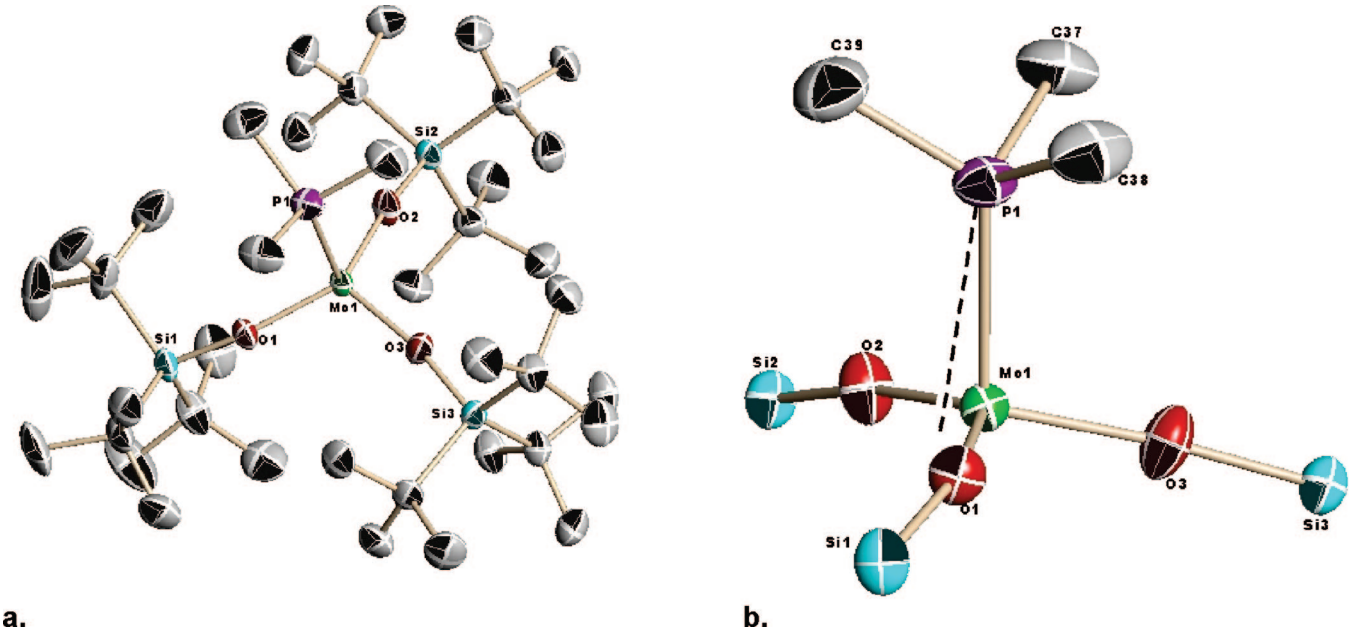

Figure 1. Molecular (a) and core (b) views of $(silox)_3MoPMe_3$ (**1**-PMe_3) showing MoP cant toward open ∠OMoO of 132.71(7)° and off-axis orientation of PMe_3.

from the geometry in the crystal structure. Its orbital energies are indicated in Figure 3, but those of the "less squashed" structure are in close correspondence. The fact that two independent molecules in the crystal structure lead to independent minima in the calculated versions supports the inference that the free energy surface for these species is

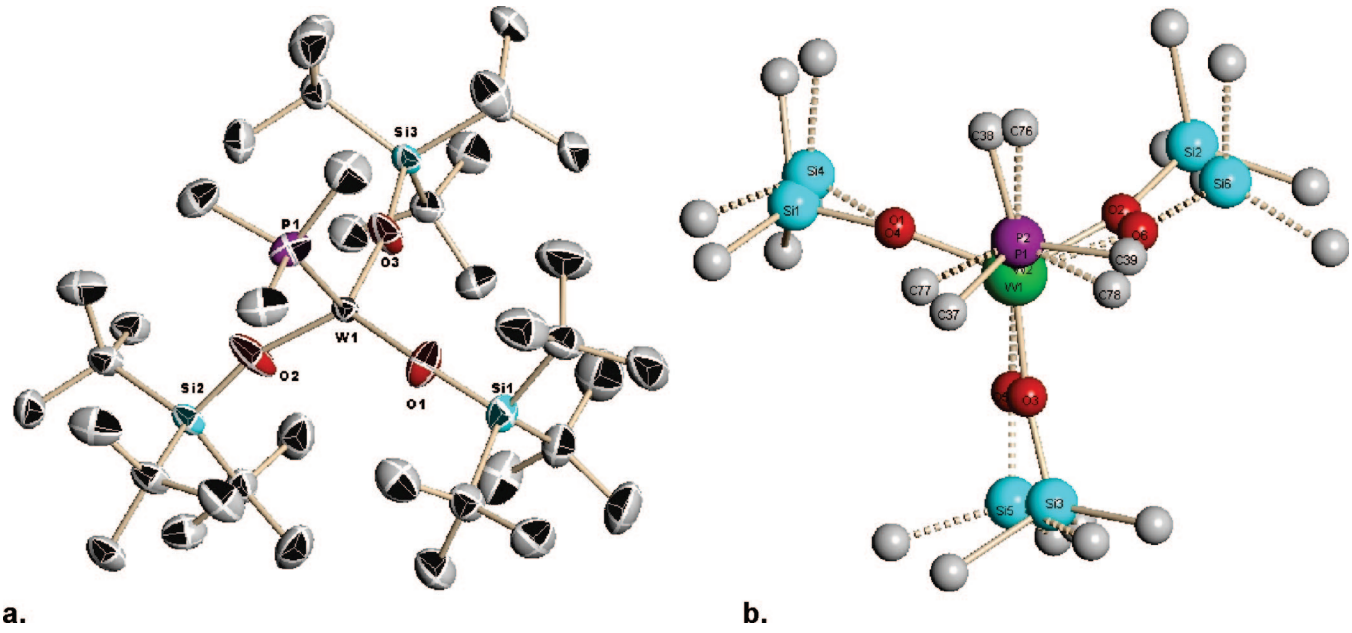

Figure 2. Molecular view (a) of the less symmetric (W1-containing) molecule of $(silox)_3WPMe_3$ (**2**-PMe_3). The cores of the two independent molecules are shown (b) such that W1/W2, P1/P2, and O1/O4 overlap.

likely to be very flat, and perhaps containing numerous conformational minima.

While care should be taken to compare the Mo vs W orbital energies, the energy dispersion (2.34 ev) in W is slightly greater than Mo (2.07 eV) as expected for a slightly greater ligand field strength for the third row element.[19] The distortion from C_{3v} symmetry is marginally more substantial (d_{xz}/d_{yz} splitting $\approx$ 0.89 eV) for W, which is expected on the basis of slightly greater $5d_{z^2}/6s$ mixing that would enable greater d_{z^2}/d_{xz} (σ/π) mixing, as previously discussed. The general orbital discussion above for Mo also applies to W. Unlike its Mo counterpart, the quartet geometry for ^{4}**2′**-PMe_3 is very similar to the doublet geometry even though it is 10.7 kcal/mol higher in energy. This is again consistent with more effective σ/π-mixing for tungsten, which would also permit ready distortion from the C_{3v} trigonal monopyramidal geometry seen for $^4(silox)_3MoPMe_3$ (^{4}**1′**-PMe_3).

Reactivity of $(silox)_3MPMe_3$. 1. $(silox)_3MoPMe_3$ (1-PMe_3). While the d^3 phosphine complexes are structurally related, subtle differences in their electronic features affect their reactivity patterns. Thermolysis of $(silox)_3MoPMe_3$ (**1**-PMe_3) in the solid state under vacuum (130°, 24 h, 10^{-3} torr) produced green $(silox)_3Mo$ (**1**) in virtually quantitative yield, as illustrated in Scheme 2. Structural characterization by single crystal X-ray methods was hampered by insoluble twinning problems; the same situation exists for $(silox)_3Ta$. Variable temperaure magnetic susceptibility measurements on **1** shown in Figure 4 reveal a μ_{eff} of 3.3 μ_B from 40−300 K that is consistent for an $S = {}^3/_2$ species possessing a modest orbital contribution. At low temperatures, μ_{eff} declines to ~2.0 μ_B as zero-field splitting effects become apparent.[19] Concentration independent solution molecular weight measurements corroborate the monomeric (M_r(calc) = 742, M_r(found) = 870(140)) formulation of **1**.

The magnetism and molecular weight measurements are consistent with a $^4A_2'$ ground-state of pseudotrigonal $(silox)_3Mo$ (**1**). Hybrid DFT/MM calculations[20−25] performed on ^{4}**1′** corroborate the proposed trigonal structure, and the classic a_1' ($d_{z^2}{}^1$), e" ($d_{xz}{}^1d_{yz}{}^1$), and e′ ($d_{x^2-y^2}$, d_{xy}) ordering is reproduced

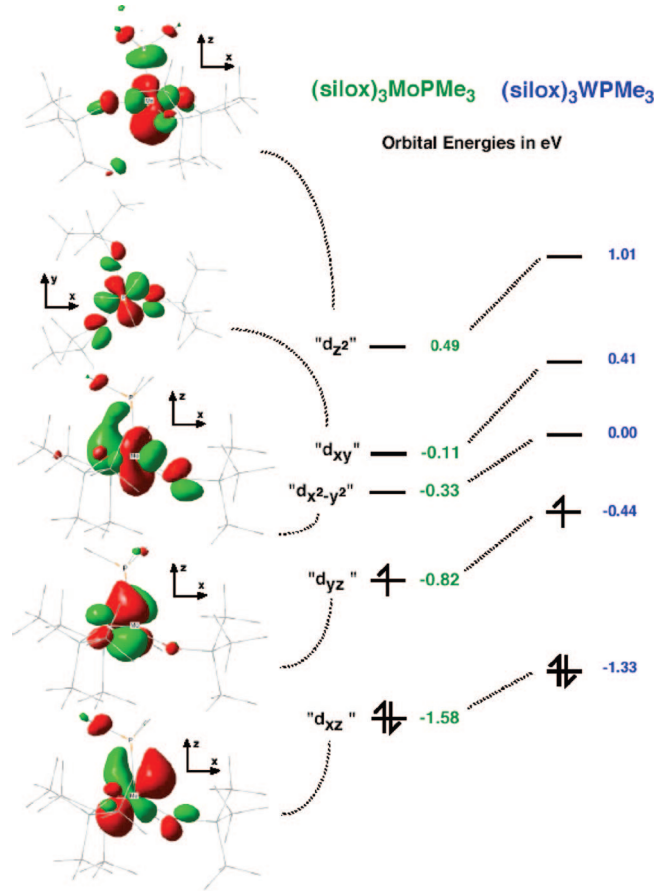

Figure 3. Ligand field orbital energies (eV) for $(silox)_3MoPMe_3$ (^{2}**1′**-PMe_3, green) and $(silox)_3WPMe_3$ (^{2}**2′**-PMe_3, blue). The orbitals illustrated are those of ^{2}**1′**-PMe_3; the orbitals for ^{2}**2′**-PMe_3, which correspond to the model of the W2-containing structure, are similar. Consider the xy plane to be that containing the P, the metal and O3 for Mo and O5 for W.

in the d-orbital splitting diagram derived from the calculations (Figure 5). The lowest orbital ($d_{z^2}{}^1$) is essentially nonbonding,

Scheme 2

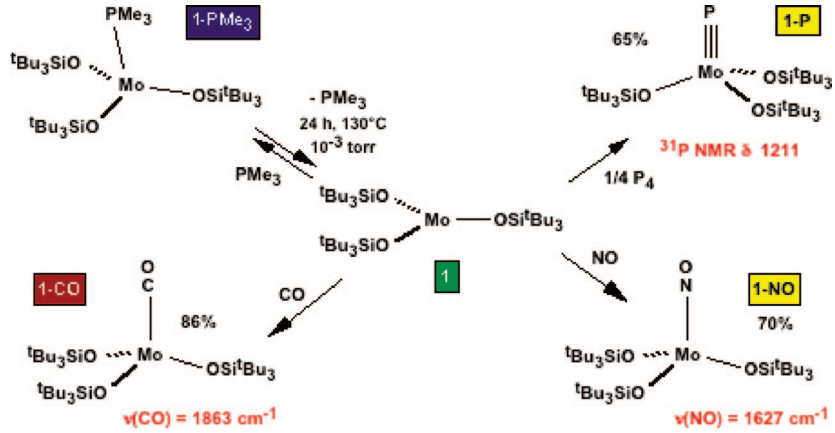

and the ($d_{xz}^1 d_{yz}^1$) set is clearly pure O→Mo π^* in character. The $d_{x^2-y^2}$, d_{xy} set reveals both σ^* and π^* character pertaining to the Mo−O bonds.

Exposure of (silox)$_3$Mo (**1**) to PMe_3 regenerated **1**-PMe_3, and suggested that adducts might be prepared in this simple fashion. In Scheme 2, **1** was treated with some common reagents in order to highlight its synthetic versatility. The red carbonyl (silox)$_3$MoCO (**1**-CO) was synthesized in 86% yield upon treatment of **1** with an excess of CO.[28] An Evans' method measurement[18] on **1**-CO afforded a μ_{eff} of 1.7 μ_B, consistent with the expected $S = {}^1/_2$ ground state, but the degree to which this complex is Jahn−Teller distorted is unknown. Formal reduction of **1** was accomplished via treatment with NO, which provided diamagnetic, yellow (silox)$_3$MoNO (**1**-NO) in 70% isolated yield. Its IR spectrum exhibited a n(NO) of 1624 cm^{-1}, which is in the range of related compounds.[29−31] Formal oxidation of **1** was accomplished via its reaction with P_4[32] to provide the yellow phosphide (silox)$_3$MoP (**1**-P) in 65% yield. The resonance for the phosphide was located at δ 1211 in its ^{31}P NMR spectrum,[33] which was significantly downfield from that of the anionic [(silox)$_3$NbP]Li (δ 790),[34,35] but very close to previous *tris*-alkoxide and *tris*-amido molybdenum compounds, such as (RO)$_3$MoP (R = adamantyl, δ 1124; 1-Me-C_6H_{10}, δ 1130)[36] and (ArNR)$_3$MoP (Ar = 3,5-$Me_2C_6H_3$, R = ^{t}Bu,[37] δ 1216, R = ^{i}Pr, δ 1256).[36,38]

2. (silox)$_3$WPMe$_3$ (2-PMe$_3$). The ready formation of (silox)$_3$Mo (**1**) due to thermal loss of PMe_3 from the (silox)$_3$MoPMe_3 (**1**-PMe_3) adduct prompted a similar approach to the synthesis of (silox)$_3$W (**2**). Unfortunately, despite significant effort, no tractable W compound(s) could be isolated using this approach, although free PMe_3 was noted. NMR tube and small scale experiments of (silox)$_3$WPMe_3 (**2**-PMe_3) with 1 equiv NO revealed the presence of (silox)$_3$WNO (**2**-NO),[1] but the substitution process was not clean, and the nitrosyl was only observed in ~55% yield by a ^{1}H NMR spectroscopic assay. The carbonyl derivative, (silox)$_3$WCO (**2**-CO) was cleanly prepared by substitution, and the yellow phosphide (silox)$_3$WP (**2**-P) was generated via addition of 1/4 equiv P_4 in 55% yield (Scheme 3). Strong evidence for **2**-P was obtained from the ^{31}P NMR spectrum that exhibited a single resonance at δ 909 with tungsten satellites (^{183}W, I = 1/2, 14.3%) indicative of J_{WP} = 162 Hz. The data correlate well with structurally characterized tungsten phosphides {(^{i}Pr)(3,5-Me_2-C_6H_3)N}$_3$WP (δ 1021, J_{WP} = 193 Hz)[39] and {N($CH_2CH_2NSiMe_3$)$_3$}WP (δ 1080, J_{WP} = 138 Hz).[40] Note that the comparative NMR shifts (and that of the Mo complexes above) may be construed as reflecting the π-bonding characteristics of O- vs N-donors. The orientation of the amides in the Cummins and Schrock tungsten-phosphides renders their π-bonding limited to the "xy" plane, whereas the siloxides in **2**-P can donate into d_{xz} and d_{yz}, thereby mixing some W−O antibonding character into predominantly WP bonding orbitals. In corroboration, note that Scheer's low temperature characterization of (^{t}BuO)$_3$WP (δ 845, J_{WP} = 176 Hz) suggests that it similar to **2**-P.[41,42]

While (silox)$_3$WPMe_3 (**2**-PMe_3) can be used as a W(III) source, its difficult synthesis prompted attempts at alternative preparations of the derivatives. Consequently, the carbonyl and nitrosyl were synthesized via Na/Hg reductions of adducts (silox)$_3$WCl(L) (**2**-ClL; L = CO, NO). As previously described, the nitrosyl could only be isolated in ~95% purity in 24% yield due to the complication of various redistribution reactions that occur during reduction. (silox)$_3$WNO (**2**-NO) has a ν(NO) of

(28) Peters, J. C.; Odom, A. L.; Cummins, C. C. *Chem. Commun.* **1997**, 1995–1996.
(29) (a) Cherry, J. P. F.; Johnson, A. R.; Baraldo, L. M.; Tsai, Y. C.; Cummins, C. C.; Kryatov, S. V.; Rybak-Akimova, E. V.; Capps, K. B.; Hoff, C. D.; Haar, C. M.; Nolan, S. P. *J. Am. Chem. Soc.* **2001**, *123*, 7271–7286. (b) Agapie, T.; Odom, A. L.; Cummins, C. C. *Inorg. Chem.* **2000**, *39*, 174–179.
(30) Blackmor, I. J.; Jin, X.; Legzdins, P. *Organometalllics* **2005**, *24*, 4088–4098.
(31) Hayton, T. W.; Legzdins, P.; Sharp, W. B. *Chem. Rev.* **2002**, *102*, 935–991.
(32) Stephens, F. H.; Johnson, M. J. A.; Cummins, C. C.; Kryatov, O. P.; Kryatov, S. V.; Rybak-Akimova, E. V.; McDonough, J. E.; Hoff, C. D. *J. Am. Chem. Soc.* **2005**, *127*, 15191–15200.
(33) Wu, G.; Rovnyak, D.; Johnson, M. J. A.; Zanetti, N. C.; Musaev, D. G.; Morokuma, K.; Schrock, R. R.; Griffin, R. G.; Cummins, C. C. *J. Am. Chem. Soc.* **1996**, *118*, 10654–10655.
(34) Hirsekorn, K. F.; Veige, A. S.; Wolczanski, P. T. *J. Am. Chem. Soc.* **2006**, *128*, 2192–2193.
(35) Figueroa, J. S.; Cummins, C. C. *Dalton Trans.* **2006**, 2161–2168.
(36) Stephens, F. H.; Figueroa, J. S.; Diaconescu, P. L.; Cummins, C. C. *J. Am. Chem. Soc.* **2003**, *125*, 9264–9265.
(37) Laplaza, C. E.; Davis, W. M.; Cummins, C. C. *Angew. Chem., Int. Ed. Engl.* **1995**, *34*, 2042–2044.
(38) Cherry, J.-P. F.; Stephens, F. H.; Johnson, M. J. A.; Diaconescu, P. L.; Cummins, C. C. *Inorg. Chem.* **2001**, *40*, 6860–6862.
(39) Fox, A. R.; Clough, C. R.; Piro, N. A.; Cummins, C. C. *Angew. Chem., Int. Ed.* **2007**, *46*, 973–976.
(40) Zanetti, N. C.; Schrock, R. R.; Davis, W. M. *Angew. Chem., Int. Ed.* **1995**, *34*, 2044–2046.
(41) Scheer, M.; Kramkowski, P.; Schuster, K. *Organometallics* **1999**, *18*, 2874–2883.
(42) (a) Balazs, G.; Gregoriades, L. J.; Scheer, M. *Organometallics* **2007**, *26*, 3058–3075. (b) Johnson, B. P.; Balazs, G.; Scheer, M. *Coord. Chem. Rev.* **2006**, *250*, 1178–1195.

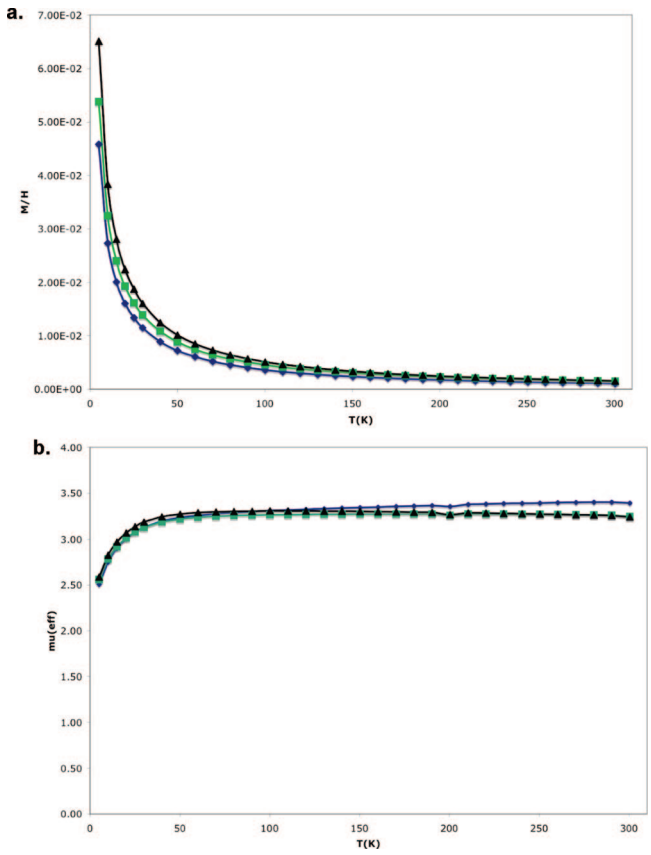

Figure 4. Overlaid M/H vs T (a) and corresponding μ_{eff} vs T (b) plots, each pertaining to an independently prepared sample (3) of $(silox)_3Mo$ (**1**).

1574 cm^{-1} in its IR spectrum, and is diamagnetic; its deoxygenation to give the nitride $(silox)_3WN$ was the subject of a study focusing on the orbital symmetry requirements for oxygen atom transfer (OAT).[1] The greater backbonding to the nitrosyl in W vs Mo is likely to be a consequence of the greater radial extension of 5d-orbitals for π-bonding, and stronger σ-bonding with a more energetically accessible $5d_{z^2}$.

Treatment of $(silox)_3WCl$ (**2**-Cl) with 1 equiv CO produced a paramagnetic red $(silox)_3ClWCO$ (**2a**-ClCO) complex with a silox resonance at δ 5.95 ($\nu_{1/2}$ = 2.3 Hz) in its ^1H NMR spectrum. Over the course of 7 d, a new paramagnetic resonance at δ 6.05 ($\nu_{1/2}$ = 2.3 Hz) grew in at the expense of the first, giving evidence of a second isomer of $(silox)_3ClWCO$ (**2b**-ClCO). The latter isomer could be made directly from **2**-Cl and 2 equiv CO, suggesting that free CO facilitated the isomerization of **2a**-ClCO to **2b**-ClCO. An IR spectrum of **2b**-ClCO revealed a ν(CO) of 1986 cm^{-1}, and its $^{13}C\{^1H\}$ NMR spectrum exhibited resonances at δ 45.47 and δ 219.00 for the silox methyl groups and tertiary carbons, respectively, along with a resonance at δ 271.72 for the CO (from a ^{13}CO sample). On this basis it is difficult to predict the structure of **2b**-ClCO given the proclivity of 5-coordinate complexes to undergo rapid rearrangement. Reduction of **2b**-ClCO with Na/Hg in DME afforded orange-red $(silox)_3WCO$ (**2**-CO) in 52% yield; paramagnetic **2**-CO was characterized by a ν(CO) of 1818 cm^{-1} in its IR spectrum, a single silox resonance at δ −0.87 ($\nu_{1/2}$ = 26 Hz) in the ^1H NMR spectrum, and a solution μ_{eff} of 1.7 μ_B.

Structure of $(silox)_3WCO$ (2-CO). Carbonyls $(silox)_3MCO$ (M = Mo, **1**-CO; W, **2**-CO) are d^3-adducts related to the phosphines $(silox)_3MPMe_3$ (M = Mo, **1**-PMe_3; W, **2**-PMe_3), but the CO ligand has substantially weaker σ-donating and better π-backbonding capabilities. If π-effects were the principal cause of the distortions in the phosphine complexes, perhaps the carbonyls would be similarly affected, but if σ-effects were the most important component, it is likely that the carbonyls would not be as severely Jahn−Teller distorted. A single crystal X-ray structural study of **2**-CO was conducted to probe the change from PMe_3 to CO in terms of the core geometry of $(silox)_3ML$.

Details of the data collection on $(silox)_3WCO$ (**2**-CO) can be found in Table 1, while its metric parameters can be found in Table 2. As Figure 6 illustrates, **2**-CO is a very modestly distorted trigonal monopyramid, consistent with a ^2E ground state (C_{3v}).[19] Its core features O−W−O angles of 111.25(11)°, 113.26(11)° and 117.63(11)°, and C−W−O angles of 101.88(14)°, 105.46(13)°, and 105.85(14)°. The subtle O−W−O angular distortion may be typical for X_3M Jahn−Teller systems; $[(silox)_3Cr]^-$ manifests a related, greater Jahn−Teller distortion that is neither T- or Y-shaped, but of a (120+α)°, 120°, and (120-α)° nature.[9] The CO does not "lean" toward either of the wider O−W−O angles but essentially away from the smaller angle (111.25(11)°) and in line with W−O3, which also possesses the widest W−O−Si angle of 172.2(2)°, thus steric factors may also be at play given the modest magnitude of the distortion from 3-fold symmetry.

The d(WO) of 1.881(12) Å (ave) are slightly shorter than those of the corresponding phosphine complex, presumably due to its decreased core electron density relative to $(silox)_3WPMe_3$ (**2**-PMe_3). The d(WC) is 1.892(4) Å is accompanied by an elongated d(CO) of 1.174(5) Å, in agreement with the significant backbonding indicated by IR spectroscopy. It is clear that the structural comparison of **2**-PMe_3 and **2**-CO corroborates the calculational finding that the W−P σ-interaction is the critical energetic factor in the extreme distortion of the former. In comparison, the d^4 $1A_1$ $(silox)_3ReCO$ complex exhibits metric parameters that can be considered a regular trigonal monopyramid.[10]

Discussion

$(silox)_3MPMe_3$ (M = Mo, 1-PMe_3; W, 2-PMe_3). In low coordinate environments, only sterically restrictive ligands can keep Mo(III) and W(III) from plunging into the thermodynamic sink accorded the metal−metal triple bond. Only the *tris*-anilide frameworks employed by Cummins et al. and the silox ligands herein have been able to stabilize mononuclear, 3- and 4-coordinate molybdenum(III) complexes,[43] and $(silox)_3WPMe_3$ is unique. The steric features of the $^tBu_3SiO$ (silox) ligand have previously been reported to help stabilize low coordinate, monomeric Ti(III), V(III), Ta(III), Cr(II), and Cr(III) as $[(silox)_3M]^n$ (n = 0, M = Ti,[7] V,[1] Ta,[1,8] Cr; n = −1, M = Cr),[9] and Nb(III) and Re(III) as $(silox)_3ML$ (M = Nb, L = PMe_3, 4-picoline;[1] Re, L = CO, PMe_3).[10]

It is also becoming evident that electronic aspects of the siloxide ligand can be critical to how effective the ligand stabilizes low oxidation states in low coordinate environments. In group 5, d^2 $(silox)_3Ta$ is relatively stable to cyclometalation, whereas "$(silox)_3Nb$" appears to exist only as a transient en route to $(silox)_2HNb(\kappa$-O,C-$OSi^tBu_2CMe_2CH_2)$.[1] The stabilization of $5d_{z^2}$ due to extensive mixing with the 6s orbital renders the S = 0 GS of $(silox)_3Ta$ stable, whereas $4d_{z^2}$ is close in energy to $4d_{xz}$ and $4d_{yz}$ in "$(silox)_3Nb$", and the nearby triplet excited states

(43) (a) Cummins, C. C. *Chem. Commun.* **1998**, 1777–1786. (b) Cummins, C. C. *Angew. Chem., Int. Ed.* **2006**, *45*, 862–870.

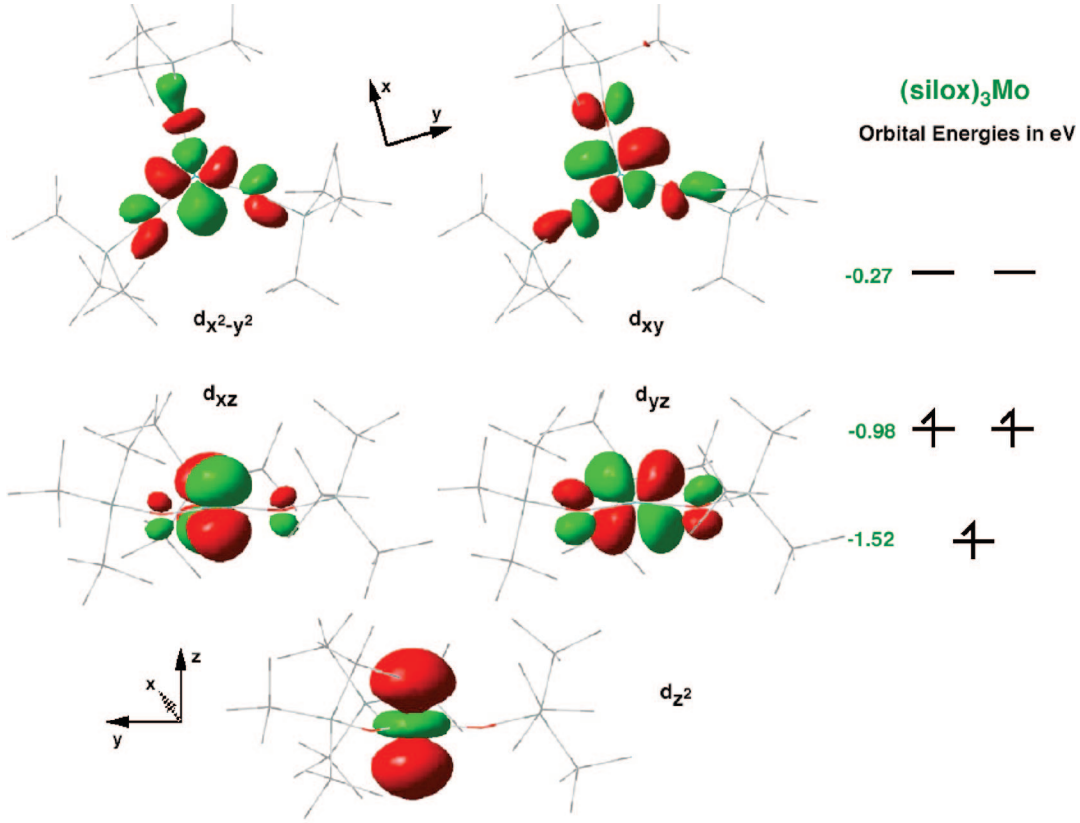

Figure 5. d-Orbitals and energies pertaining to calculated pseudotrigonal ^{4}(silox)$_3$Mo (^{4}**1′**).

Scheme 3

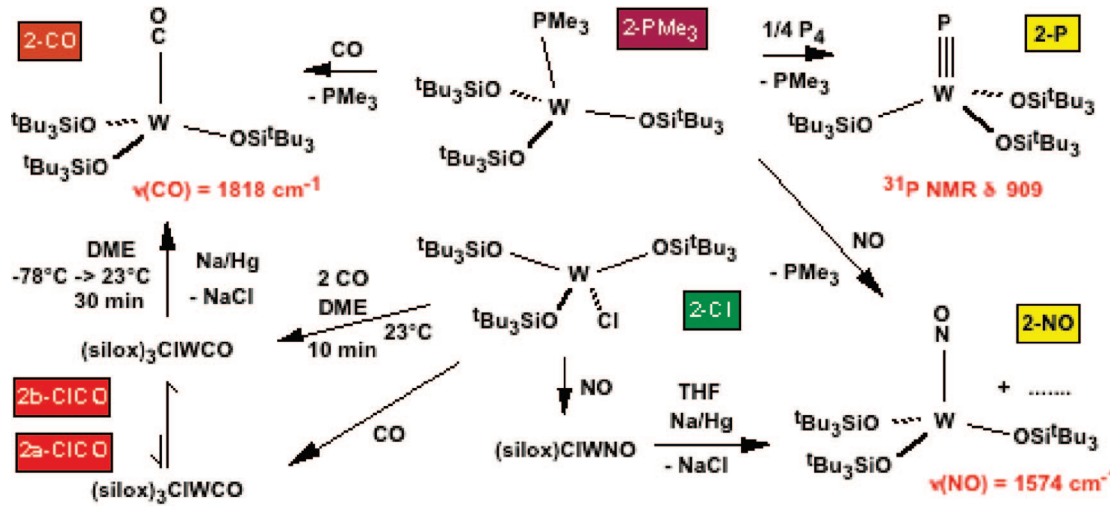

of this species facilitate binding by L, or CH-binding leading to cyclometalation. The related stabilization of 5d$_{z^2}$ in W as compared to the 4d$_{z^2}$ of Mo is critical to the squashed tetrahedral geometries found for (silox)$_3$WCl (**2**-Cl) and (silox)$_3$WMe in contrast to the trigonal monopyramidal configurations found for (silox)$_3$MoCl (**1**-Cl) and (silox)$_3$MoEt.[3]

Computationally, it is worthwhile to examine the features of (silox)$_3$MPMe$_3$ (M = Mo, **1′**-PMe$_3$; W, **2′**-PMe$_3$) with regard to the dissociation of PMe$_3$ and the relative stabilities of the putative first-formed products, (silox)$_3$M (M = Mo, **1′**; W, **2′**). Figure 7 reveals comparative enthalpy and free energy diagrams pertaining to the loss of phosphine from **1′**-PMe$_3$ vs **2′**-PMe$_3$.

Two features of the enthalpy comparison are striking. First, the tungsten ^{2}**2′**-PMe$_3$ state is significantly lower in energy than the quartet, whereas the quartet of the molybdenum PMe$_3$ complex is only a few kcal/mol above ^{2}**1′**-PMe$_3$. Recall that ^{4}**1′**-PMe$_3$ has a different geometry - that of a trigonal monopyramid,[26] hence the doublet ground-state is clearly in line with experiment. Second, the (silox)$_3$M spin state configurations are reversed. For Mo (**1′**), the quartet is lower than ^{2}**1′** by 6.0 kcal/mol, whereas the doublet is lower for W (**2′**) by 6.7 kcal/mol. The GS ^{2}**2′** geometry is highly distorted, with one O−W−O angle of 136° and the others measuring 110° and 113°. One would not predict a Jahn−Teller distortion from a trigonal

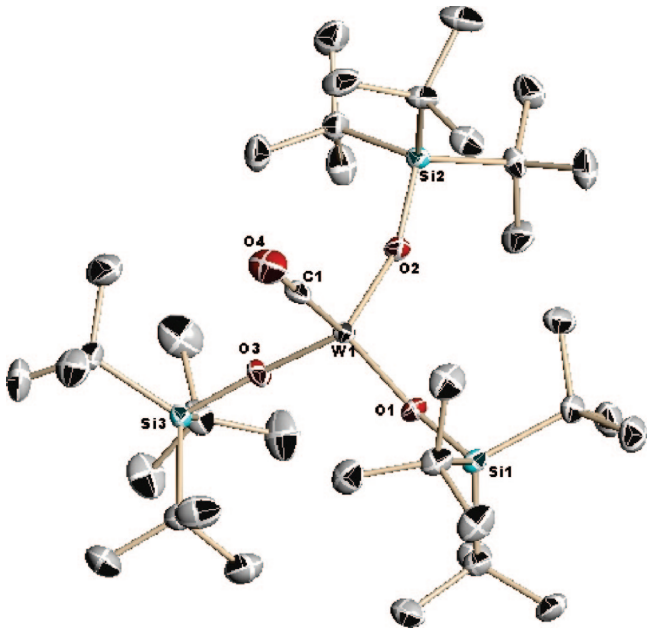

Figure 6. Molecular view of $(silox)_3WCO$ (**2**-CO).

$(silox)_3W$ fragment (i.e., the likely GS is $^4A_2'$ in D_{3h}) unless $5d_{z^2}$ is low enough to overcome a spin-pairing energy, which would lead to an orbitally degenerate $^2E''$ GS in D_{3h}. Calculations of $^2\mathbf{2}'$ place the d-orbital orderings as (in eV): (d_{z^2}),^{2} −2.1; (d_{yz}),^{1} −0.73; d_{xz}, −0.68; d_{xy}, 0.22; $d_{x^2-y^2}$, 0.27. Since the distortion only splits the e'' and e′ sets 0.05 eV, $5d_{z^2}$ is ∼1.4 eV below the $d_{xz}d_{yz}$ set, whereas $4d_{z^2}$ is only 0.54 eV below the e'' set for the molybdenum analogue, $^4\mathbf{1}'$ (Figure 5). The quartet state ($^4\mathbf{2}'$) is calculated to be ∼0.3 eV (6.7 kcal/mol) above $^2\mathbf{2}'$, and assuming similar core orbital energies, the pairing energy for the doublet state is estimated to be 1.1 eV (1.4 eV = pairing energy). A related analysis for $^4\mathbf{1}'$ and $^2\mathbf{1}'$ from Figure 5 gives the pairing energy for $(4d_{z^2})^2$ as ∼0.8 eV. Mo and W pairing energies are expected to be roughly the same, and given the crude assumptions, the values are reasonable. It is clear that d_{z^2} plays the crucial role in the determining the GS energies and configurations of $(silox)_3M$ (M = Mo, **1**′; W, **2**′), which supports preceding arguments that suggest $5d_{z^2}$ mixing with $5d_{xz}$ is more substantial than in molybdenum for the $(silox)_3MPMe_3$ (M = Mo, $^{4/2}\mathbf{1}'$-PMe_3; W, $^{4/2}\mathbf{2}'$-PMe_3) complexes.

Phosphine binding to $(silox)_3M$ (M = Mo, $^4\mathbf{1}'$; W, $^2\mathbf{2}'$) is roughly the same for both metals (−15.2 kcal/mol for Mo; −13.5 kcal/mol for W), although the Mo case requires an intersystem crossing.[1,44−46] The free energy picture of phosphine dissociation overestimates the ease of PMe_3 loss, since the PMe_3 adducts are stable in solution and $(silox)_3Mo$ (**1**) rapidly scavenges 1 equiv PMe_3. Moreover, the GS of $(silox)_3MoPMe_3$ (**1**-PMe_3) is a doublet, not the quartet as calculated. Nonetheless, the free energy picture suggests that dissociative loss of PMe_3 is not difficult from a thermodynamic standpoint, so it is likely to be the instability of the doublet GS of $(silox)_3W$ ($^2\mathbf{2}'$) that prevents its isolation. As a corollary, the intrinsic stability of

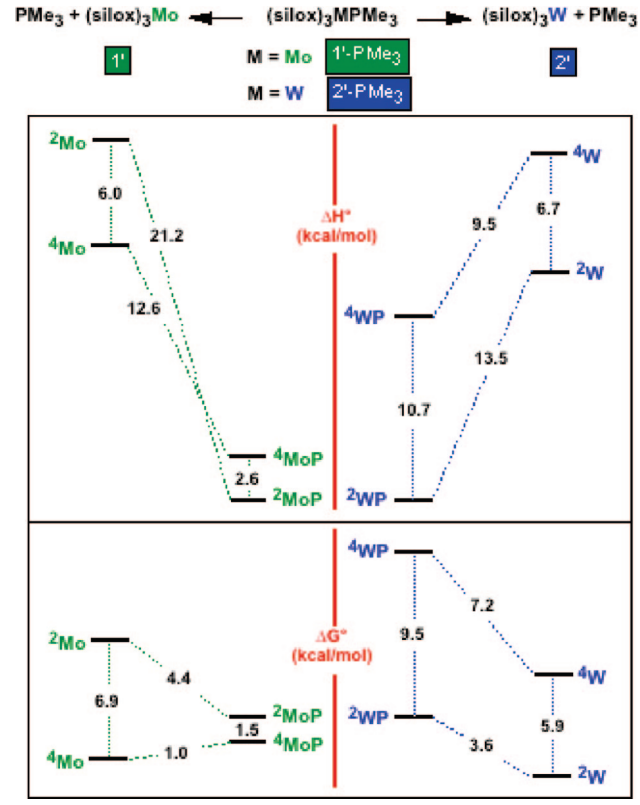

Figure 7. Calculated standard enthalpies (top) and free energies (bottom) for PMe_3 dissociation from $^{4/2}(silox)_3MPMe_3$ (M = Mo, **1**′-PMe_3; W, **2**′-PMe_3) to $^{4/2}(silox)_3M$ (M = Mo, **1**′; W, **2**′) + PMe_3. The $^2(silox)_3MPMe_3$ models are arbitrarily set to equal energies in each case for ready comparison.

the quartet state of $(silox)_3Mo$ ($^4\mathbf{1}'$) may inhibit detrimental degradation paths. As a consequence of the low lying, filled $5d_{z^2}$ orbital, $^2\mathbf{2}'$ has a relatively low-lying empty d_{xz} orbital that can serve as an acceptor to nucleophilic substrates, or CH bonds that ultimately can oxidatively add, such as in the cyclometalation of a silox[1] or PMe_3 ligand. The equivalent event for molybdenum would require a promotional energy for access to $^2\mathbf{1}'$, suggesting an additional kinetic barrier. Parkin has recently provided nice examples of the relatively greater proclivity of W(II) to add CH bonds in comparison to analogous Mo(II) species.[47] It is expected that paths leading to W(V) products from $^2\mathbf{2}'$ are likely to be operative and would hamper isolation of $(silox)_3W$ (**2**), whereas the possibility of generating Mo(V) products from CH bond activation and related reactions are not likely to be thermodynamically viable.

$(silox)_3Mo$ (1). Historically, a number of Mo(III) species containing alkoxide, siloxide, and other pseudohalide ligands have represented a critical area of coordination chemistry—that of MoMo triple bonds.[6] While the stability of the quartet GS of $(silox)_3Mo$ (**1**) has been discussed above with the aid of computation, history suggests that the stability of this configuration is not enough to prevent dimerization. It appears that the steric features of $^tBu_3SiO$ are once again critical to the isolation of this low-coordinate, low-valent complex.[48] In order

(44) (a) Poli, R. *J. Organomet. Chem.* **2004**, *689*, 4291–4304. (b) Poli, R. *Acc. Chem. Res.* **1997**, *30*, 1861–1866.
(45) (a) Harvey, J. N.; Poli, R.; Smith, K. M. *Coord. Chem. Rev.* **2003**, *238*, 347–361. (b) Poli, R.; Harvey, J. N. *Chem. Soc. Rev.* **2003**, *32*, 1–8. (c) Harvey, J. N.; Poli, R. *Dalton Trans.* **2003**, 4100–4106.
(46) (a) Harvey, J. N. *Struc. and Bond.* **2004**, *112*, 151–183. (b) Harvey, J. N. *Phys. Chem. Chem. Phys.* **2007**, *9*, 331–343.
(47) (a) Buccella, D.; Tanski, J. M.; Parkin, G. *Organometallics* **2007**, *26*, 3275–3278. (b) Buccella, D.; Parkin, G. *J. Am. Chem. Soc.* **2006**, *128*, 16358–16364. (c) Churchill, D. G.; Janak, K. E.; Wittenberg, J. S.; Parkin, G. *J. Am. Chem. Soc.* **2003**, *125*, 1403–1420.
(48) Hahn, J.; Landis, C. R.; Nasluzov, V. A.; Neyman, K. M.; Rösch, N. *Inorg. Chem.* **1997**, *36*, 3947–3951.

Table 3. Dimerization of (silox)Mo (**1**) is Prevented by Steric Factors

$$^{1}(R^{1}{}_{2}R^{2}EO)_3Mo \equiv Mo(OER^{1}{}_{2}R^{2})_3 \overset{\Delta H^\circ_{rxn} = BDE}{\rightleftharpoons} 2\ ^{4}(R^{1}{}_{2}R^{2}EO)_3Mo$$

	BDE (kcal/mol)	d(MoMo) (Å)	∠ O−Mo−O (°)
E = C; $R^1 = R^2 =$ Me	60	2.29	118
E = Si; R^1 = Me, $R^2 = {}^t$Bu	88	2.30	117
E = Si; $R^1 = {}^t$Bu, R^2 = Me	60	2.41	114
E = Si; $R^1 = R^2 = {}^t$Bu	(−93)	2.89	108

Table 4

eq	calculated dinitrogen cleavage by ^{4}(silox)$_3$Mo (**1′**)	$\Delta H°$ (kcal/mol)	$\Delta S°$ (cal/K-mol)	$\Delta G°$ (kcal/mol)
1	^{4}(silox)$_3$Mo + N_2 ⇌ ^{2}(silox)$_3$Mo−NN	−9.3	−38.6	2.2
2	^{2}(silox)$_3$Mo−NN + ^{4}(silox)$_3$Mo ⇌ ^{3}(silox)$_3$Mo−NN−Mo(silox)$_3$	−45.9	−79.7	−22.1
3	2 ^{4}(silox)$_3$Mo + N_2 ⇌ ^{3}(silox)$_3$Mo−NN−Mo(silox)$_3$	−55.2	−118.3	−20.0
4	^{3}(slox)$_3$Mo−NN−Mo(silox)$_3$ ⇌ 2 ^{1}(silox)$_3$MoN	−14.1	56.0	−30.8
5	2 ^{4}(silox)$_3$Mo + N_2 ⇌ 2 ^{1}(slox)$_3$MoN	−69.3	−62.4	−50.7

to check on the veracity of a purely steric argument, the bond dissociation enthalpies (BDEs) and d(MoMo) were calculated for a series of dimolybdenum triple bonded species.

As Table 3 indicates, a strong case can be made that dimerization of (silox)Mo (**1**) is prevented by steric factors. The calculated d(MoMo) and ∠O−Mo−O for (^{t}BuO)$_3$MoMo(O^{t}Bu)$_3$ and (^{t}BuMe$_2$SiO)$_3$MoMo(OSiMe$_2{}^t$Bu) are in accord with related complexes whose structures have been determined.[6] The MoMo bond strength of the siloxide complex is somewhat greater than the *tert*-butoxide derivative, presumably because stronger π-donation from the latter adds antibonding character to the dimolybdenum unit. As steric factors are increased by replacement of Me with ^{t}Bu, the triple bond lengthens by >0.1 Å, the BDE correspondingly weakens, and the ⟨O−Mo−O decreases.[48] The hypothetical compound of interest, ^{1}(silox)$_3$MoMo(silox)$_3$ (**1′**$_2$) is calculated to be in a shallow local minimum that is 93 kcal/mol above separated ^{4}(silox)$_3$Mo (**1′**) fragments. It has an exceptionally long d(MoMo) of 2.89 Å and is essentially tetrahedral about Mo, whereas the true dimolybdenum species are roughly trigonal monopyramidal.[26] It is clear that the silox ligand is sterically prohibitive regarding dimolybdenum bond formation, given the large, negative ΔH_{rxn} ("BDE") calculated for dissociation.

The related *tris*-anilide species of Cummins et al. (i.e., (ArN^{t}Bu)$_3$Mo, Ar = 3,5-Me$_2$C$_6$H$_3$) cleaves dinitrogen over extended periods to give (ArN^{t}Bu)$_3$MoN via (ArN^{t}Bu)$_3$MoN$_2$ and [(ArN^{t}Bu)$_3$Mo]$_2$N$_2$.[47−49] Orbital symmetry problems associated with a linear dissociation are obviated by "kinking" the MoNNMo linkage, and a "zigzag" transition state has been proposed to facilitate σ/π-mixing to permit the scission.[49−53] Since (silox)$_3$Mo (**1**) has electronic features similar to (ArN^{t}Bu)$_3$Mo, calculations were conducted to address the thermodynamic feasibility of N_2 cleavage, even though dinitrogen binding and/or activation has not been observed.

As Table 4 indicates, 2 equiv (silox)$_3$Mo (**1′**) are capable of cleaving dinitrogen to the corresponding nitride (silox)$_3$MoN (**1′**-N), since the enthalpy and free energy changes are −69 and −51 kcal/mol, respectively. The values are slightly less favorable than Morukuma's model[52] of the *tris*-anilide molybdenum system, which is 2 (H$_2$N)$_3$Mo + N_2 → 2 (H$_2$N)$_3$MoN ($\Delta E \approx \Delta H = -74$ kcal/mol). However, while initial dinitrogen binding to ^{4}**1′** is exothermic (−9 kcal/mol), it is slightly endoergic (2 kcal/mol). The related binding of N_2 to (H$_2$N)$_3$Mo is calculated to be exothermic by ∼ −18 kcal/mol, although the overall conversion to the bridging dinitrogen species, (H$_2$N)$_3$MoNNMo(NH$_2$)$_3$ is almost identical (−54 kcal/mol)[52] to the value given in eq 3. Since the π-donation of amide ligands has been promoted by Morokuma as a strong factor in the initial binding of N_2 to (H$_2$N)$_3$Mo,[52] perhaps the attenuated π-donating ability of the siloxides lessens the capability of the Mo center to π-backbond to the dinitrogen in ^{2}**1′**-N$_2$. Solutions of (silox)$_3$Mo (**1**) incur no color change when placed under 1 atm N_2, and neither do ^{1}H NMR spectra of **1** change upon exposure to dinitrogen. The calculations, which suggest N_2 binding to be borderline observable, are therefore within reason of experiment. Note that there is a change to low spin upon N_2 binding to **1′**, and this is accompanied by a structural change as elaborated on for ^{2}(silox)$_3$MoPMe$_3$ (^{2}**1′**-PMe$_3$). A reorganizational energy is likely to be a penalty to N_2 binding due to the structural change, so there may also be a substantial barrier for N_2 adduct formation.

A related change in spin accompanies attachment of the second ^{4}**1′** to ^{2}**1′**-N$_2$ although this process occurs with $\Delta G° = -22$ kcal/mol, and a $\Delta H°$ of −46 kcal/mol. The aforementioned "zigzag" transition state would be required for dinitrogen cleavage from ^{3}(silox)$_3$MoNNMo(silox)$_3$ (^{3}**1′**$_2$-N$_2$), providing another substantive barrier for dissociation to 2 **1′**-N.[49,52] Transition states were not addressed in these calculations, so there is no direct information regarding the highest barrier in the overall N_2 binding/cleavage process, but the lack of an observable dinitrogen complex (e.g., ∼−30 °C and 1 atm N_2 for extended periods), and comparison with Morokuma's calculations of the *tris*-anilide system, suggests that it is the initial binding event that is most problematic. Redox-catalysis of N_2 cleavage by (silox)$_3$Mo (**1**) has not been attempted,[50,51] nor have high pressures been explored.

Molybdenum(III) and Tungsten(III). A search of the literature for mononuclear examples of Mo(III) and W(III) species revealed surprisingly few examples for comparison. The vast

(49) (a) Laplaza, C. E.; Johnson, M. J. A.; Peters, J. C.; Odom, A. L.; Kim, E.; Cummins, C. C.; George, G. N.; Pickering, I. J. *J. Am. Chem. Soc.* **1996**, *118*, 8623–8638. (c) Figueroa, J. S.; Piro, N. A.; Clough, C. R.; Cummins, C. C. *J. Am. Chem. Soc.* **2006**, *128*, 940–950.
(50) Curley, J. J.; Cook, T. R.; Reece, S. Y.; Müller, P.; Cummins, C. C. *J. Am. Chem. Soc.* **2008**, *130*, 9394–9405.
(51) Peters, J. C.; Cherry, J.-P. F.; Thomas, J. C.; Barlado, L.; Mindiola, D. J.; Davis, W. M.; Cummins, C. C. *J. Am. Chem. Soc.* **1999**, *121*, 10053–10067.
(52) Cui, Q.; Musaev, D. G.; Svensson, M.; Sieber, S.; Morokuma, K. *J. Am. Chem. Soc.* **1995**, *117*, 12366–12367.
(53) Neyman, K. M.; Nasluzov, V. A.; Hahn, J.; Landis, C. R.; Rosch, N. *Organometallics* **1997**, *16*, 995–1000.

majority of non metal−metal bonded compounds are 6-coordinate (counting Cp and related ligands as tridentate), and no W(III) mononuclear species comparable to $(silox)_3WPMe_3$ were found. The only legitimately comparable Mo(III) species are the *tris*-amide and *tris*-amidoamine derivatives of Cummins et al. and Schrock et al., respectively. As previously discussed with regard to dinitrogen and P_4 activation, $(ArNR)_3Mo$ species possess a wealth of remarkable reactivity.[41] Related 5-coordinate complexes, such as $\{[RNCH_2CH_2]_3N\}MoL$ have also exhibited some fascinating chemistry, such as the reduction of N_2 to NH_3 in the presence of judicious H^+ sources combined with reducing agents. In the latter case R is the extremely bulky aryl 3,5-(2,4,6-^{i}Pr$_3$C$_6$H$_2$)$_2$C$_6$H$_3$,[54,55] whereas earlier R = TMS or C_6F_5 versions of the "tren" ligand[56] proved to be the scaffolds for low valent derivatives $\{[Me_3SiNCH_2CH_2]_3N\}MoL$ (L = N_2,[57] CO, C_2H_4, CNR) and $\{[C_6F_5NCH_2CH_2]_3N\}WCO$.[58]

Conclusions

The steric and electronic features of the ^{t}Bu$_3$SiO (silox) ligand have proven capable of enabling the synthesis of low coordinate, low valent d^3 $(silox)_3ML$ (M = Mo, **1**-L; W, **2**-L; *L* = PMe_3, CO) and $(silox)_3Mo$ (**1**). The PMe_3 adducts **1**-PMe_3 and **2**-PMe_3 feature two distinct distortions from 3-fold symmetry. A distortion leads to a squashed-T_d geometry for the core of each molecule, and significant σ/π mixing in the low symmetry (C_s) revealed by a bent M-P bond[12] suggests that it is not a simple Jahn−Teller case. $5d_{z^2}/6s$ mixing in the third row lowers the energy of $5d_{z^2}$ to a greater degree than $4d_{z^2}$ is lowered in second row transition metal species, thereby providing a crucial electronic contrast between W and Mo. The effects are not readily discerned in the GS doublet **1**-PMe_3 and **2**-PMe_3 complexes, but the greater doublet/quartet energy gap for the latter is a probable consequence. The stability of quartet $(silox)_3Mo$ (**1**) with respect to its more reactive doublet state can be attributed to its relatively high energy $4d_{z^2}$ orbital, whereas putative $(silox)_3W$ (**2**) is calculated to be doublet state subject to Jahn−Teller distortion. The doublet GS of **2**, which has a low lying empty orbital that can serve as an electron acceptor, in combination with the greater thermodynamic inclination of W(III) to oxidize, is proposed as the reason why the three-coordinate tungsten species could not be isolated. At the origin of these differences is the relativistic contraction of s and p shells in concert with the radial expansion and energetic destabilization (due to increased screening) of d and f shells in third row transition metals.[5] These cases can also be considered specific variations in sd^n hybridization as a function of row, and corroborate valence bond concepts of Landis et al.[4]

Experimental Section

General Considerations. All manipulations were performed using either glovebox or high vacuum line techniques. Hydrocarbon solvents containing 1−2 mL of added tetraglyme, and ethereal solvents were distilled under nitrogen from purple sodium benzophenone ketyl and vacuum transferred from same prior to use. Benzene-d_6 was dried over activated 4 Å molecular sieves, vacuum transferred and stored under N_2. All glassware was oven-dried, and NMR tubes for sealed tube experiments were additionally flame-dried under dynamic vacuum. Gaseous reagents (CO, NO; Matheson) were used as received and passed over a −78 °C trap prior to use. $(silox)_3MoCl$ (**1**-Cl), $(silox)_3ClMoPMe_3$ (**1**-ClPMe_3), $(silox)_3WCl$ (**2**-Cl),[3] and $(silox)_3WNO$ (**2**-NO)[1] were prepared according to literature procedures.

NMR spectra were obtained using Varian XL-400, INOVA-400, and Unity-500 spectrometers, and chemical shifts are reported relative to benzene-d_6 (^{1}H, δ 7.15; ^{13}C{^{1}H}, δ 128.39). Infrared spectra were recorded on a Nicolet Impact 410 spectrophotometer interfaced to a Gateway PC. Solution magnetic measurements were conducted via Evans' method in C_6D_6 unless otherwise noted.[18] Elemental analyses were performed by Oneida Research Services (Whitesboro, NY) or Robertson Microlit Laboratories (Madison, NJ).

Procedures. 1. $(silox)_3MoPMe_3$ (1-PMe_3). To a 50 mL round-bottom flask equipped with a stir bar was added 1.50 g of $(silox)_3MoCl$ (**1**-Cl, 1.76 mmol), 4.68 g of Na/Hg (0.95% Na, 1.93 mmol Na), and 25 mL of Et_2O. After the transfer of 2.0 equiv of PMe_3 via gas bulb, the reaction mixture was stirred at 23 °C. Over 24 h, the reaction mixture changed to a deep-purple color. All volatiles were removed from the reaction mixture, and the mercury was decanted. Pentane (∼30 mL) was distilled into the flask, and the reaction mixture was filtered and stripped of all volatiles to give a purple solid. The purple solid was dissolved in minimal Et_2O, and the resulting solution was allowed to slowly evaporate at −30 °C (∼18 h) to give large purple blocks of **1**-PMe_3 after decantation of the mother liquor (0.94 g, 65% yield). ^{1}H NMR (C_6D_6): δ 1.51 ($\nu_{1/2} \approx$ 20 Hz, 27H, C(C*H*$_3$)), 2.62 ($\nu_{1/2} \approx$ 48 Hz, 3H, P(C*H*$_3$)$_3$). ^{13}C{^{1}H} NMR (C_6D_6): δ 39.09 (C(*C*H$_3$)), 137 (SiC). Anal. Calcd for $C_{39}H_{90}O_3PSi_3Mo$: C, 57.24; H, 11.09. Found: C, 56.96; H, 10.82. μ_{eff} (293K) = 2.0 μ_B.

2. $(silox)_3WPMe_3$ (2-PMe_3). a. $(silox)_3ClWPMe_3$ (2-ClPMe_3). To a 25 mL flask was added 400 mg of $(silox)_3WCl$ (**2**-Cl, 0.461 mmol) and 8 mL of PMe_3 by vacuum transfer at −78 °C. The resulting blue suspension was warmed to 23 °C and stirred for 3 h. Filtration at −78 °C afforded 362 mg (83%) of a light-blue precipitate, **2**-ClPMe_3. ^{1}H NMR (C_6D_6, tentative due to insolubility): at δ 2.31 ($\nu_{1/2}$ = 18 Hz, 27 H, C(CH$_3$)$_3$), δ 5.31 ($\nu_{1/2}$ = 11 Hz, 54 H, C(CH$_3$)$_3$), PMe_3 not observed.

b. 2-PMe_3. To a 100 mL flask was added 709 mg of **2**-ClPMe_3 (0.830 mmol), 1.94 g of Na/Hg (0.936%, 0.872 mmol Na), and 50 mL of Et_2O via vacuum transfer at −78 °C. The reaction mixture was stirred at 23 °C for 40 h, and the solution changed from blue-green to brown. All volatiles were removed from the reaction mixture, and the Hg was decanted. Pentane (∼30 mL) was distilled into the flask, and the reaction mixture was filtered and stripped of all volatiles to give a brown solid. The solid was dissolved in 10 mL of a 10:1 Et_2O:PMe_3 mixture and cooled to −40 °C for 24 h to afford 283 mg of crystalline burgundy **2**-PMe_3 (41%). ^{1}H NMR (C_6D_6): δ 1.31 ($\nu_{1/2} \approx$ 37 Hz, 81 H, C(C*H*$_3$)), 12.77 (tentative, $\nu_{1/2} \approx$ 950 Hz, ∼5 H, P(C*H*$_3$)$_3$). ^{13}C{^{1}H} NMR (C_6D_6): δ 38.45 (C(*C*H$_3$)). Anal. Calcd for $C_{39}H_{90}O_3PSi_3Mo$: C, 51.63; H, 10.11. Found: C, 51.21; H, 9.88. μ_{eff} (293K) = 1.7 μ_B.

3. $(silox)_3Mo$ (1). To a 50 mL round-bottom flask fitted with a 180° needle valve was added 1.00 g of $(silox)_3MoPMe_3$ (**1**-PMe_3, 1.22 mmol) that had been ground to a fine powder. The purple powder was heated to 150 °C for 4 h under dynamic vacuum (10^{-3}−10^{-4} torr) to give a light-green powder (0.86 g, 95% yield). ^{1}H NMR (C_6D_6): δ 2.51 ($\nu_{1/2} \approx$ 76 Hz). ^{13}C{^{1}H} NMR (C_6D_6): δ 173 (br, CH$_3$), 268 (SiC). Anal. Calcd for $C_{36}H_{81}O_3Si_3Mo$: C, 58.26; H, 11.00. Found: C, 57.97; H, 10.71. μ_{eff} (293K) = 3.0 μ_B (see Figure 4).

4. $(silox)_3MoCO$ (1-CO). To a 25 mL round-bottom flask equipped with a stir bar was added 0.200 g of $(silox)_3Mo$ (**1**, 0.269 mmol) and 10 mL of Et_2O. The green solution was exposed to 10 equiv of CO, which was transferred via calibrated gas bulb. A dark red-brown solid formed immediately. The reaction mixture was

(54) (a) Yandulov, D. V.; Schrock, R. R. *Science* **2003**, *301*, 76–78. (b) Yandulov, D. V.; Schrock, R. R. *Inorg. Chem.* **2005**, *44*, 1103–1117.
(55) Byrnes, M. J.; Dai, X.; Schrock, R. R.; Hock, A. S.; Müller, P. *Organometallics* **2005**, *24*, 4437–4450.
(56) Schrock, R. R. *Acc. Chem. Res.* **1997**, *30*, 9–16.
(57) O'Donoghue, M. B.; Davis, W. M.; Schrock, R. R. *Inorg. Chem.* **1998**, *37*, 5149–5158.
(58) Greco, G. E.; O'Donoghue, M. B.; Seidel, S. W.; Davis, W. M.; Schrock, R. R. *Organometallics* **2000**, *19*, 1132–1149.

stirred for an additional hour and then filtered at −78 °C to give 0.176 g **1**-CO (85%). ^{1}H NMR (C_6D_6): δ 1.52 ($\nu_{1/2} \approx 10$ Hz, 81H, C(C*H*$_3$)). ^{13}C{^{1}H} NMR (C_6D_6): δ 30.13 (SiC), 35.71 (CH_3). IR (Nujol mull, Na/Cl, cm^{-1}) 1863 (ν(CO)). Anal. Calcd for $C_{37}H_{81}O_4Si_3Mo$: C, 57.70; H, 10.60. Found: C, 57.52; H, 10.41. μ_{eff} (293K) = 1.7 μ_B.

5. (silox)$_3$MoNO (1-NO). To a 25 mL round-bottom flask equipped with a stir bar was added 0.200 g (silox)$_3$Mo (**1**, 0.269 mmol) and 10 mL Et$_2$O. The green solution was cooled to −78 °C and exposed to 10 equiv NO, which was transferred via calibrated gas bulb. The reaction mixture was warmed to 23 °C, and the solution turned yellow-orange. After 1 h of stirring, the solution was concentrated to ∼2 mL, cooled to −78 °C, and filtered to give 0.166 g of canary yellow **1**-NO (80%). ^{1}H NMR (C_6D_6): δ 1.26 (C*H*$_3$). ^{13}C{^{1}H} NMR (C_6D_6): δ 23.47 (SiC), 29.66 (CH_3). IR (Nujol mull, Na/Cl, cm^{-1}) 1627 (ν(NO)). Anal. Calcd for $C_{36}H_{81}NO_4Si_3Mo$: C, 55.99; H, 10.57; N, 1.81. Found: C, 55.69; H, 10.32; N, 1.80.

6. (silox)$_3$MoP (1-P). To a 4-dram vial containing 0.200 g (silox)$_3$Mo (0.269 mmol) in 5 mL Et$_2$O at 23 °C was added 12 mg P_4 (0.094 mmol). As the reaction mixture stirred at 23 °C for 4 h, the color changed to a deep reddish brown. Evaporation of the Et$_2$O at −30 °C for 12 h gave fine yellow needles of **1**-P which were collected by filtration (0.135 g, 65%). ^{1}H NMR (C_6D_6): δ 1.35 (s, 81H, C(C*H*$_3$)). ^{13}C{^{1}H} NMR (C_6D_6): δ 24.63 (*C*(CH$_3$)), 30.82 (C(*C*H$_3$)). ^{31}P NMR (C_6D_6): δ 1211 (s). Anal. Calcd for $C_{36}H_{81}O_3PSi_3Mo$: C, 55.92; H, 10.56. Found: C, 55.72; H, 10.47.

7. (silox)$_3$W(CO)Cl (2-ClCO). To a 25 mL flask charged with (silox)$_3$WCl (**2**-Cl, 300 mg, 0.347 mmol) was distilled 10 mL of benzene at −78 °C. Two equivalents of CO (estimated from flask headspace volume) were added, and the flask was warmed to 23 °C. A deep-red solution developed as the benzene thawed, and after 10 min of stirring, the volatiles were removed to afford a red solid. A ^{1}H NMR assay revealed **2**-ClCO contaminated by 1−2% of (silox)$_3$WCl$_2$,[3] and 1−2% of (silox)$_3$WCO (**2**-CO). ^{1}H NMR (C_6D_6): δ 6.05 ($\nu_{1/2} \approx 2.3$ Hz, C(C*H*$_3$)). ^{13}C{^{1}H} NMR (C_6D_6): δ 45.47 (C(*C*H$_3$)), 219.00 (*C*(CH$_3$)), 217.72 (^{13}CO). IR (Nujol mull, Na/Cl, cm^{-1}) 1986 (ν(CO)). Anal. Calcd for $C_{37}H_{81}O_4Si_3W$: C, 49.73; H, 9.14. Found: C, 49.90; H, 8.97.

8. (silox)$_3$WCO (2-CO). To a 25 mL flask charged with a (silox)$_3$WCl(CO) (**2**-ClCO, 430 mg, 0.481 mmol) and 1.5 equiv of Na/Hg (0.50% Na, 11.6 mg, 0.505 mmol Na, 2.32 g Hg) was added 15 mL DME by distillation at −78 °C. The reaction mixture slowly warmed to 23 °C, and the solution became dark orange over the course of 30 min. The volatiles were removed, and the solid was triturated with pentane (2 × 15 mL), taken up in 15 mL of pentane, and filtered. The solution was reduced to ∼9 mL and cooled to −78 °C to afford a dark-orange powder that was collected by filtration. Recrystallization from pentane provided 214 mg of crude **2**-CO (∼52%). ^{1}H NMR analysis of the orange solid indicated a 90% purity, with 4% **2**-Cl and 1% (silox)$_3$WCl$_2$[3] identifiable; no EA was attempted. ^{1}H NMR (C_6D_6): δ −0.87 ($\nu_{1/2} \approx 26$ Hz, CH_3)). IR (Nujol mull, Na/Cl, cm^{-1}) 1818 (ν(CO)). μ_{eff} (293K) = 1.7 μ_B.

9. (silox)$_3$WP (2-P). To a 25 mL flask charged with 7 mg (0.06 mmol) of P_4 and 204 mg (0.225 mmol, 4 equiv) of (silox)$_3$WPMe$_3$ (**2**-PMe$_3$) was added 10 mL of Et$_2$O via vacuum transfer at −78 °C. The reaction was allowed to slowly warm to room temperature over 30 min and then stirred for an additional 3.5 h. During this time, the solution lightened from dark brown to deep yellow. The reaction mixture was then filtered and the solvent reduced to 3 mL, cooled to −78 °C, and then filtered to afford 97 mg (50%) of a yellow powder. ^{1}H NMR (C_6D_6): δ 1.34 (s, C(C*H*$_3$)). ^{13}C{^{1}H} NMR (C_6D_6): δ 24.89 (SiC), 31.22 (C(*C*H$_3$)$_3$). ^{31}P NMR (C_6D_6): δ 908.83 (J_{WP} = 162 Hz). Anal. Calcd for $C_{36}H_{81}O_3PSi_3W$: C, 50.21; H, 9.48. Found: C, 49.96; H, 9.85.

NMR Tube Reactions. 10. 2-PMe$_3$ + CO. A J-Young tube was charged with 23 mg of **2**-PMe$_3$ (0.025 mmol), and 0.5 mL of C_6D_6 was added. The tube was freeze−pump−thaw degassed three times on the vacuum line, and 1 atm (excess) of CO was admitted. Upon thawing, the solution had changed from brown to dark orange and ^{1}H NMR spectroscopic analysis indicated quantitative conversion to (silox)$_3$WCO (**2**-CO) and 1 equiv of free PMe$_3$.

11. 2-PMe$_3$ + NO. A J-Young tube was charged with 26 mg of **2**-PMe$_3$ (0.029 mmol), and 0.5 mL of C_6D_6 was added. The tube was freeze−pump−thaw degassed three times on the vacuum line, and 1.1 equiv of NO was added via a calibrated gas bulb. Upon thawing, the solution lightened to lemon-yellow and some yellow precipitate formed. ^{1}H NMR analysis indicated ∼55% conversion to (silox)$_3$WNO (**2**-NO) among other products. Adding NO to a cold (−78 °C) pentane solution of **2**-PMe$_3$ and allowing to slowly warm to 23 °C did not affect the product distribution.

Single Crystal X-Ray Diffraction Studies. Upon isolation, the crystals were covered in polyisobutylene and placed under a 173 °C N_2 stream on the goniometer head of a Siemens P4 SMART CCD area detector system (graphite-monochromated Mo Kα radiation, λ = 0.71073 Å). The structures were solved by direct methods (SHELXS). All non-hydrogen atoms were refined anisotropically unless stated, and hydrogen atoms were treated as idealized contributions (Riding model).

12. (silox)$_3$MoPMe$_3$ (1-PMe$_3$). A dark purple-brown block (0.4 × 0.3 × 0.2 mm) was obtained from diethyl ether. A total of 46 866 reflections were collected with 11 388 determined to be symmetry independent (R_{int} = 0.0481), and 8500 were greater than 2σ(*I*). The data was corrected for absorption by SADABS, and the refinement utilized $w^{-1} = \sigma^2(F_o^2) + (0.0458p)^2 + 3.7714p$, where $p = (F_o^2 + 2F_c^2)/3)$.

13. (silox)$_3$WPMe$_3$ (2-PMe$_3$). A dark-burgundy block (0.2 × 0.2 × 0.2 mm) was obtained from diethyl ether. A total of 144395 reflections were collected with 31033 determined to be symmetry independent (R_{int} = 0.0478), and 21805 were greater than 2σ(*I*). The data was corrected for absorption by SADABS, and the refinement utilized $w^{-1} = \sigma^2(F_o^2) + (0.0336p)^2 + 1.0782p$, where $p = (F_o^2 + 2F_c^2)/3)$. Disordered solvent was SQEEZd out of the model, and one of the two independent molecules has a disordered silox group.

14. (silox)$_3$WCO (2-CO). A red needle (0.75 × 0.1 × 0.09 mm) was obtained from slow evaporation of a hexanes solution. A total of 27578 reflections were collected with 10176 determined to be symmetry independent (R_{int} = 0.0351), and 8656 were greater than 2σ(*I*). The data was corrected for absorption by SADABS, and the refinement utilized $w^{-1} = \sigma^2(F_o^2) + (0.0529p)^2 + 0.0p$, where $p = (F_o^2 + 2F_c^2)/3)$.

Computational Methods. Calculations were performed on full silox-decorated models using the Gaussian03 package.[20] Density functional theory (DFT), specifically the BLYP functional, was utilized for all simulations.[21] The transition metals and heavy main group atoms (Si and P) were described with the Stevens effective core potentials (ECPs) and attendant valence basis sets (VBSs).[22] This scheme, dubbed CEP-31G, entails a valence triple-ζ description for the transition metals, and a double-ζ VBS for the main group elements. The 6−31G(d) all-electron basis set was used for C, H and O atoms. All main group VBSs are augmented with a d polarization function (C(ξ_d) = O(ξ_d) = 0.8; Si(ξ_d) = 0.3247; P(ξ_d) = 0.37). This level of theory was selected on the basis of a series of test calculations on the singlet and triplet states of Nb(OH)$_3$, Ta(OH)$_3$,[1] and their olefin adducts.[23]

Full silox models were studied using hybrid quantum mechanics/molecular mechanics (QM/MM) techniques within the ONIOM framework.[24] The QM region of M(silox)$_3$(X) complexes contained the transition metal, the O and Si atoms of the silox group, and the entire X group (if present). The QM level of theory employed is that described above. The remainder of the molecule, that is, the *tert*-butyl groups of silox, was modeled with the Universal Force Field (UFF).[25]

Full geometry optimizations without any metric or symmetry restrictions were employed to obtain the minima in this research. All of the resultant stationary points were characterized as true minima (i.e., no imaginary frequencies) by calculation of the

energy Hessian. Enthalpic and entropic corrections to the total electronic energy were calculated using harmonic vibrational frequencies determined at the same level of theory employed for geometry optimization and are calculated at 1 atm and 298.15 K.

Closed- and open-shell species were described with the restricted and unrestricted Kohn−Sham formalisms, respectively, with no evidence of spin contamination for the latter.

Acknowledgment. We thank the National Science Foundation (CHE-0415506, (P.T.W.)), the U.S. Dept. of Energy (DE-FG02-03ER15490 (T.R.C.)), and Cornell University for financial support. Elliott B. Hulley, LeGrande M. Slaughter, and Adam S. Veige are thanked for experimental assistance.

Supporting Information Available: CIF file (**1**-PMe_3, CCDC 660936; **2**-PMe_3, CCDC 660938; **2**-CO), and complete ref 20. This material is available free of charge via the Internet at http://pubs.acs.org.

JA802706U